ACS OMEGA

Open Access

http://pubs.acs.org/journal/acsodf

Article

Theoretical Study of Am(III) and Eu(III) Separation by a Bipyridyl Phosphate Ligand

Xinyi Zhang, Lulu Ye, Weihao Chen, Xiaofei Zhang, Weiwei Chen, Miaogen Chen,* and Pinwen Huang*

Cite This: *ACS Omega* 2024, 9, 12060−12068

Read Online

ACCESS | Metrics & More | Article Recommendations | Supporting Information

ABSTRACT: Actinide An(III) and lanthanide Ln(III) are known to exhibit similar chemical properties; thus, it is difficult to distinguish them in the separation of highly radioactive waste liquids. One potential method to efficiently separate actinides and lanthanides involves the design and development of phosphorus−oxygen-bonded ligands with solvent extraction separation. Here, a bipyridine phosphate ligand with two isopropyl and phosphate groups is introduced to selectively extract actinides. The electronic structure, bonding properties, thermodynamic behavior, and quantum theory of atoms in molecules (QTAIM) of Am(III) and Eu(III) complexes with the bipyridine phosphate ligands were analyzed by using density functional theory (DFT) calculations. The analysis demonstrates that the Am−N bond exhibits stronger covalent characteristics than the Eu−N bond, indicating that the bipyridine phosphate ligand had better selectivity for Am(III) than for Eu(III) in terms of binding affinity. The thermodynamic analysis established the complex $[ML(NO_3)_2(H_2O)_2]^+$ as the most stable species during the complexation process. The results indicate great potential for utilizing the bipyridine phosphate ligand for the effective separation of An(III)/Ln(III) in spent fuel reprocessing experiments.

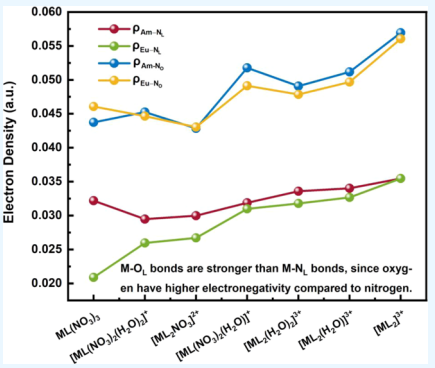

1. INTRODUCTION

To promote the development of a low-carbon economy, fossil energy is gradually being replaced by various green and nonpolluting novel energy sources. Among them, nuclear energy is considered a key solution for addressing the energy crisis due to its cost-effectiveness and environmental friendliness. However, nuclear energy sources generate a large amount of nuclear waste, classified by radioactivity intensity into high-level waste (HLW), low-level waste, and intermediate-level waste.[1] HLW, also known as spent fuel, primarily comes from nuclear fuel after combustion in nuclear power plants.[2] The reprocessing of HLW plays a pivotal role in the nuclear fuel cycle, essential not only for reducing nuclear waste but also for mitigating the environmental hazards posed by radioactive wastes, ensuring sustainable advancement of nuclear energy.[3,4] To address this challenge, the international strategy of partition and transmutation (P&T) was proposed in the 1970s, which involves the separation/partition of minor actinides (MA) and long-lived fission products (LLFP) and converting them from high toxicity to low toxicity.[5,6]

It has been hypothesized that the complete removal of MA could reduce the final waste volume in subterranean repositories by a factor of 100, reducing the required size of repositories by a factor of 5 in comparison to those needed for open nuclear fuel cycle plans.[7] However, the separation of MA, which requires a solvent extraction process capable of extracting small amounts of actinides (An) from the nitric acid solution, presents a significant challenge due to the chemical similarities in the ionic radii, oxidation states, parallel electrostatics, and spatial site resistance factors in solution, especially the An(III)/Ln(III).[8−10]

To achieve the efficient extraction of An(III), several candidate extractants have been proposed (Figure 1). Bis-triazinyl-pyridine (BTP), composed solely of carbon (C), hydrogen (H), oxygen (O), and nitrogen (N), is a promising candidate extractant that exhibits excellent performance and generates no secondary waste.[11,12] 6,6′-Bis(5,5,8,8-tetramethyl-5,6,7,8-tetrahydro-benzol[1,2,4]triazin-3-yl)[2,2]bipyridine (CyMe4-BTBP) is another effective extractant known for its resistance to acidic environments and the intense radiation of radiolysis present during the separation.[13,14] Additionally, 2,9-bis(5,5,8,8-tetramethyl-5,6,7,8-tetrahydro-1,2,4-benzotriazin-3-yl)-1,10-phenanthroline (CyMe4-BTPhen) possesses higher surface activity at the organic/water interface than CyMe4-BTBP due to higher local concentrations.[15] Zsabka et al. demonstrated that [A336][NO3]/CyMe4-BTPhen could be utilized either with or without a phase transfer catalyst and co-

Received: December 12, 2023
Revised: February 7, 2024
Accepted: February 14, 2024
Published: February 29, 2024

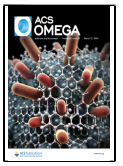

https://doi.org/10.1021/acsomega.3c09940
ACS Omega 2024, 9, 12060−12068

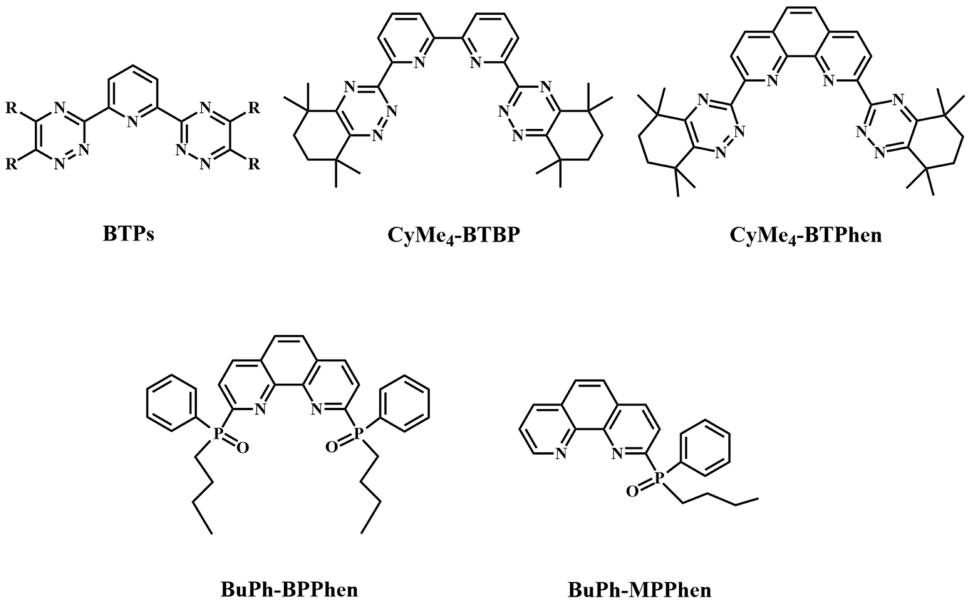

Figure 1. Structures of BTPs, CyMe4-BTBP, CyMe4-BTPhen, BuPh-BPPhen, and Bh-MPPhen.

diluent for separating actinides from lanthanide series, effectively resolving the sluggish kinetics even at elevated temperatures.[16]

For many soft N-donor and S-donor ligands, the extended actinide 5f orbitals can be distinguished from the more contracted lanthanide 4f orbitals. The covalent interaction between the soft N- or S-donor ligands and the 5f orbitals of An(III) is significantly stronger than that with the 4f orbitals of Ln(III). Xu et al. developed two novel ligands named C2-POPhen and C4-POPhen, both based on the phenanthroline phosphonate structure.[17,18]

These ligands were designed to selectively extract trivalent actinides, but not lanthanides. The ligands demonstrated high extraction efficiency but showed only moderate selectivity for trivalent actinides compared with lanthanides when tested in highly acidic nitrate solutions. Several other ligands were synthesized, such as Ph_2-BPPhen, which is a tetradentate *N,O*-heterophenanthroline phosphine oxide ligand, and BuPh-BPPhen and BuPh-MPPhen, which are 1,10-phenanthroline ligands. These ligands were developed for co-extracting trivalent f-block elements from highly radioactive liquid wastes.[19] However, it has limited solubility in typical diluents, such as octanol, and further studies are necessary to understand the coordination chemistry between f-block elements and *N,O*-hybrid phenanthroline-phosphine oxide ligands.

BuPh-BPPhen and BuPh-MPPhen show potential in successfully separating and characterizing 10 coordination lanthanide complexes of solid $EuL^1(NO_3)_3$ (BuPh-BPPhen, L^1) and $[EuL^2(NO_3)_3(H_2O)]Et_2O$ (BuPh-MPPhen, L^2). Therefore, a fresh polydentate phosphine oxide-functionalized 2,2′-bipyridine ligand was synthesized to further expand the organophosphorus extractant derived from phenanthroline and explore its potential to segregate and form complexes with trivalent lanthanides and actinides. This ligand combines the advantages of bipyridine with the O group found in the −P═O group of the TOPO-type ligand, which finds wide applications as an extractant for separating trace amounts of actinides in the TRPO process (trialkylphosphine oxide).[20] Additionally, with a structure featuring two P═O groups, this ligand has the potential to act as a tetradentate ligand, which provides a good platform to explore the effects of multi-coordination and substituents on the complexation and extraction behavior of these ligands on f-block elements.

Due to the high experimental cost caused by the high radioactivity of actinides, a computational chemistry approach has been found to be necessary to study lanthanide and actinide separation.[21] Thus, we conducted a thorough analysis of the extraction of bipyridine phosphate ligands through relativistic quantum chemical computations, examining their impact on the Am(III)/Eu(III) separation across various nitric acid solutions. The study particularly delved into several issues, including molecular structure, electrostatic potential (ESP), and the MOs model of bipyridyl phosphate ligands: structure, bonding properties, molecular MOs, and thermodynamic behavior of complexes formed by Am(III) and Eu(III) with bipyridyl phosphate ligands. The results helped expand and advance our comprehension of how bipyridyl phosphate ligands facilitate the separation of An(III)/Ln(III), which is crucial in developing novel bipyridyl phosphate ligand derivatives for elemental separation purposes. In addition, after the actinide and lanthanide extraction from aqueous phase, they can be further purified from the organic phase by back-extraction, ion-exchange resins, or specific adsorbent materials in the process of reducing nuclear waste.

2. COMPUTATIONAL METHODS

The advancement in theoretical techniques has significantly enhanced the role of computational chemistry, making it a useful tool for elucidating the extraction mechanism of N- and S-donor ligands that contain f-block elements. The calculations were performed using the Gaussian 09 software, employing the B3LYP method in density functional theory (DFT).[22−25] The B3LYP method is a hybrid density generalization combining features of the Hartree−Fock (HF) method and DFT, merging the exchange functional of Becke 88 and the three-parameter functional (B3) with the correlation functional developed by Lee, Yang, and Parr (LYP). In this theoretical calculation, Am(III) and Eu(III) represented actinides and lanthanides, respectively. To model these elements, small core pseudopo-

https://doi.org/10.1021/acsomega.3c09940
ACS Omega 2024, 9, 12060−12068

tentials (quanti-relativistic effective core potentials, RECP) were employed, specifically using ECP60MWB-SEG and ECP28MWB-SEG valence groups in a segmented contraction mode for Am and Eu. This implied that the pseudopotentials were used to replace 60 inner core electrons in Am and 28 inner core electrons in Eu.[26,27] The f-level electrons and other remaining electrons of the metal atom were treated as valence electrons for light elements like C, H, O, and N, and 6-31G(d) or 6-311G(2df,p) basis sets were used. The optimized stable systems at the B3LYP/6-31G(d)/RECP level of theory were analyzed by using vibrational frequencies. If the system frequencies were real, then each of these configurations represented a local minimum in terms of the energy on the potential energy surface.

Additionally, QTAIM analysis was conducted using Multiwfn 3.8 software to delve into the bond characteristics between metal ions and ligands at the same level of theory.[28] The NBO analysis was also carried out on the complexes of water-soluble ligands containing phosphorus−oxygen bonds with Am(III) and Eu(III) at the B3LYP//ECP60MWB-SEG/6-311G* level. This step was crucial for elucidating the electronic and bonding characteristics of these complexes. To accurately model the environment, single-point energy computations were executed in solvent environments. The solvation effect on the complexes was meticulously accounted for using the solvation model-based density (SMD) in aqueous, cyclohexanone, and nitrobenzene organic solvents.[29]

3. RESULTS AND DISCUSSION

3.1. Bipyridyl Phosphate Ligands. The bipyridine phosphate ligand was first investigated based on the bipyridine scaffold with two isopropyl and phosphate substituents (Figure 2). Figures S1 and S2 display the electrostatic potential (ESP), as well as the highest occupied molecular orbital (HOMO) and lowest unoccupied molecular orbital (LUMO) of the ligand. The ESP reflected the chemical reactivity of the molecule, which helped in understanding the intermolecular interactions, reaction sites, etc. In Figure S1, the blue region indicates the most negative position of the ESP (nucleophilic site), suggesting that the N and O1 atoms are rich in electrons, which facilitate their coordination with metal ions. Based on the principle that a 180° rotation of the molecule can coincide with the original compound, the optimized ligand structure is deduced to exhibit approximate C_2 symmetry. The energy gap between HOMO and LUMO indicates the molecule's electron transition ability from occupied to vacant orbitals, providing partial insight into its reactivity. The LUMO is known to be related to nucleophilicity and the HOMO to electrophilicity; thus, the LUMO diagram qualitatively indicated the possible reaction sites and the likelihood of atomic participation in the reaction. Therefore, the N and the O1 atoms are most likely to participate in the reaction, aligning with the ESP diagram results.

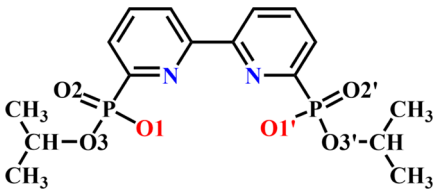

Figure 2. Structure of the bipyridine phosphate ligand.

3.2. Study of Am(III) and Eu(III) Complexes with Bipyridyl Phosphate Ligands. Previous studies have shown that trivalent actinide and lanthanide cations are highly stable in aqueous solutions and exhibit robust ionic bonding characteristics, with coordination numbers of 8 or 9 being typical in such solutions.[30] Four different hydrated metal species, $[M(H_2O)_9]^{3+}$, $[M(NO_3)(H_2O)_7]^{2+}$, $[M(NO_3)_2(H_2O)_5]^{+}$, and $M(NO_3)_3(H_2O)_3$, were optimized at the B3LYP/6-31G*/RECP level of theory to study the hydrated species in nitrate solutions. The central metal ions had coordination numbers of 9 (Figure 3).

The nitrate anion preferred to coordinate in a bidentate manner with Eu (III) and Am (III) (Figure 3), consistent with the crystal structure of $[Eu(NO_3)_3(H_2O)_3]$.[31] The complexes containing the ligands and metal ions were optimized by using the B3LYP method without any symmetry restrictions. This study focused on optimizing four separate complexes of Am(III) and Eu(III) with bipyridine phosphate ligands. Various complexes were optimized, each containing different quantities of nitrate anions and water molecules. Figure 4 shows the optimized structures of the 1:1 species $AmL(NO_3)_3$/$EuL(NO_3)_3$ and the 1:2 species $[AmL_2NO_3]^{2+}$/$[EuL_2NO_3]^{2+}$, where L stands for the bipyridine phosphate ligand. All nitrate anions coordinated in a bidentate manner

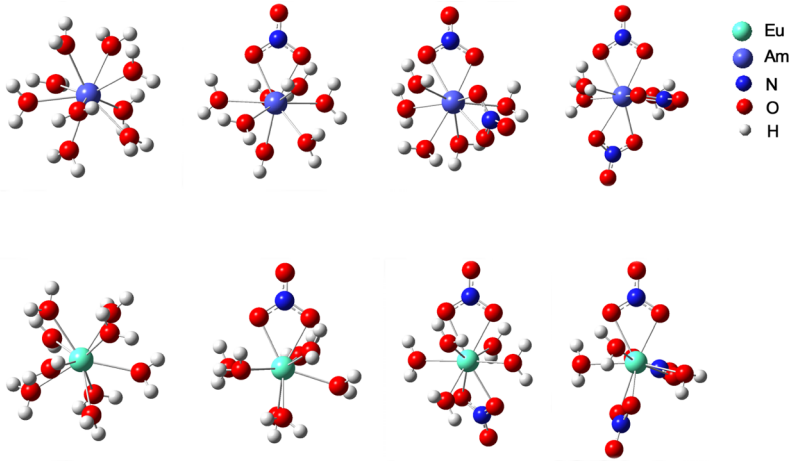

Figure 3. Optimized Am(III) and Eu(III) hydrated species were found in the gas phase.

https://doi.org/10.1021/acsomega.3c09940
ACS Omega 2024, 9, 12060−12068

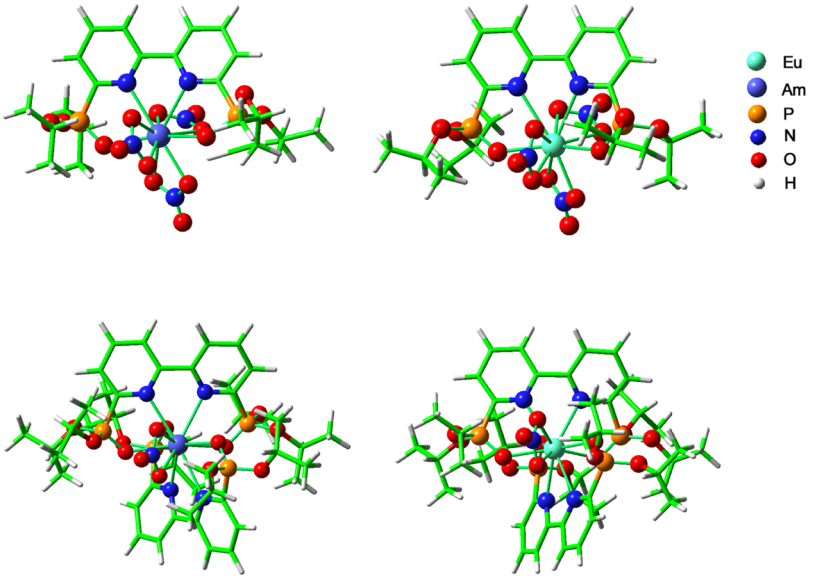

Figure 4. Optimized structures of $AmL(NO_3)_3$/$EuL(NO_3)_3$ and $[AmL_2NO_3]^{2+}$/$[EuL_2NO_3]^{2+}$ in the gas phase.

with the metal ions, resulting in central metal ion having coordination numbers between 8 and 10.[32,33]

Both the 1:1 and 1:2 species showed that the ligands were bound to Am(III) or Eu(III) ions via the N atom of the bipyridine and the O atom of the phosphate group. Table S1 shows the average bond lengths between the metal ion and the N atom in the ligand ($M-N_L$), the O atom in the nitrate group ($M-O_N$), the O atom in the water molecule ($M-O_W$), as well as the O atom in the ligand ($M-O_L$).

While certain $Am-N_L$ bond lengths were longer than those of the $Eu-N_L$ bonds, the difference did not exceed 0.06 Å (Table S1). For example, in the $[ML_2NO_3]^{2+}$ complex, the mean $Am-N_L$ bond length was 2.766 Å, which was 0.009 Å more than the $Eu-N_L$ bond length. Considering the slight variation (0.03 Å) in the radii of Am and Eu ions (r_{Am} = 0.98 Å; r_{Eu} = 0.95 Å), the Am−N bond was shorter by 0.021 Å compared to the Eu−N bond, indicating that the ligand might have interacted more strongly with Am(III) than with Eu(III).

However, in the $[ML_2]^{3+}$, $[ML_2(H_2O)]^{3+}$, $[ML_2(H_2O)_2]^{3+}$, and $[ML(NO_3)_2(H_2O)]^{+}$ complexes, the ligands interacted more strongly with Eu(III) than with Am(III). This was probably related to the relatively low concentration of nitrate in these complexes, as nitrate ions can synergistically interact with Am(III) in coordination, thereby promoting the interaction between the ligands and Am(III). The $M-N_L$ bond length typically increased when there was an increase in the number of coordinated nitrate ions (Figure 5). This may be because the more nitrate ions there are, the more crowded the cavities within the ligand become, increasing the distance between the ligand and the metal. Moreover, a higher count of nitrates in the complex led to a weaker interaction between the ligand and metal cation, indicating that the presence of more nitrate weakens the interaction between the metal ion and the ligand.

3.3. Bonding Nature. NBO analysis was performed using the B3LYP/6-311G*/RECP level of theory to obtain a better understanding of how the ligand was bonded to the central metal ion. The bonding properties of M−O and M−N bonds were examined using the Wiberg bond index (WBI) as a starting point. The WBIs have a positive correlation between

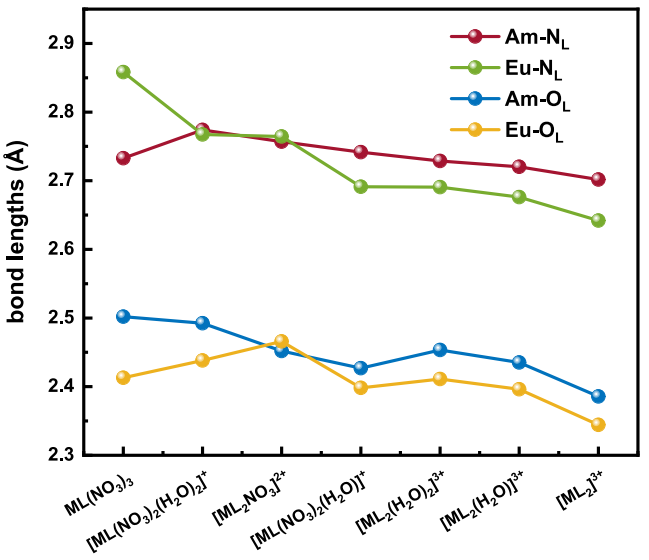

Figure 5. Variation of the calculated mean bond lengths of M−O and M−N in the Eu and Am complexes.

their size and covalent strength for the same class of bond. Table 1 shows the WBIs for M−N and M−O bonds, which, based on these calculations, were found to fall between 0.21 and 0.45. This suggested that the connection between N/O atoms and metal ions was covalent in nature but relatively weak with electrostatic interactions being more significant in $M-N_L$ and $M-O_L$ bonds. The $Am-N_L$ had a slightly higher average WBI compared to $Eu-N_L$, which implied that the bonding interaction between the nitrogen donor and Am(III) ions was stronger than that with Eu(III). For instance, in the complex $[ML(NO_3)_2(H_2O)_2]^+$, the mean WBI for the $Am-N_L$ bond was 0.335, that is, 0.122 larger than that for the corresponding Eu−N bond. These results of the WBIs study were further corroborated using Mayer bond order (MBO), which are commonly regarded as an appropriate tool for analyzing bond covalency. The calculations were extremely time-consuming and generalizable.[34] The MBOs for Am−N in the 1:1 complex $[ML(NO_3)_2(H_2O)_2]^+$ were 0.228 and 0.178

https://doi.org/10.1021/acsomega.3c09940
ACS Omega 2024, 9, 12060−12068

Table 1. WBIs of M−N and M−O Bonds (M = Am, Eu)

	$M-N_L$	$M-O_L$	$M-O_W$	$M-O_N$
$[ML_2]^{3+}$	0.246/0.287	0.338/0.432	—	
$[ML_2(H2O)]^{3+}$	0.255/0.210	0.337/0.236	0.250/0.218	
$[ML_2(H_2O)_2]^{3+}$	0.264/0.245	0.337/0.332	0.281/0.142	
$[ML_2NO_3]^{2+}$	0.225/0.235	0.322/0.340	—	0.322/0.321
$[ML(NO_3)_2(H_2O)]^{+}$	0.327/0.231	0.445/0.310	0.375/0.255	0.417/0.322
$[ML(NO_3)_2(H_2O)_2]^{+}$	0.335/0.213	0.438/0.329	0.370/0.255	0.449/0.327
$ML(NO_3)_3$	0.221/0.185	0.271/0.307	—	0.306/0.258

Table 2. MBO of M−N and M−O Bonds (M = Am, Eu)

	$M-N_L$	$M-O_L$	$M-O_W$	$M-O_N$
$[ML_2]^{3+}$	0.218/0.257	0.428/0.465	—	—
$[ML_2(H_2O)]^{3+}$	0.248/0.234	0.410/0.265	0.242/0.188	—
$[ML_2(H_2O)_2]^{3+}$	0.225/0.229	0.373/0.361	0.242/0.111	—
$[ML_2NO_3]^{2+}$	0.189/0.187	0.352/0.322	—	0.322/0.270
$[ML(NO_3)_2(H_2O)]^{+}$	0.241/0.225	0.376/0.338	0.316/0.276	0.284/0.310
$[ML(NO_3)_2(H_2O)_2]^{+}$	0.228/0.178	0.380/0.347	0.307/0.245	0.359/0.281
$ML(NO_3)_3$	0.184/0.152	0.188/0.321	—	0.273/0.274

for Eu−N, and for the 1:2 type of complex $[ML_2NO_3]^{2+}$, Am−N was 0.189 and Eu−N was 0.187 (Table 2). Thus, these results confirm that weak covalent interactions dominate the M−N and M−O bonds.

The MBO values of the Am−N bond were relatively higher than those of the Eu−N bond, indicating more pronounced covalent properties in the former. The difference in MBO values for Am−O and Eu−O was less than that for the Am−N and Eu−N bonds. Thus, the ligand exhibited an affinity for attachment to Am(III)/Eu(III) via the nitrogen atom.

These results were supported by the QTAIM method and the Multiwfn 3.8 program for the topological analysis of the nature of the bonds in the complexes.[35] Table S2 provides a summary of the calculated QTAIM parameters, including electron density (ρ), Laplace operator of electron density ($\nabla^2\rho$), electron energy density (H), |V(BCP)|/G(BCP), and energy density per unit electron at the BCP position H(r)/ρ(r). The value of QTAIM is the average of all M−N and M−O1 bonds in the complex. Multiple studies have shown that QTAIM possesses the ability to offer comprehensive insight into the bonding properties of actinide complexes. Based on these parameters, all of the electron densities were found to be below 0.10 au, and their associated Laplace operators were non-negative. Figure 6 illustrates that all $M-O_L$ bonds were stronger than $M-N_L$ bonds, primarily because oxygen had a higher electronegativity compared to that of nitrogen. Compared with other complexes, the electron density of $M-N_L$ of $ML(NO_3)_3$ is quite different, which may be because the system is neutral and more stable, and the interaction between metal and ligand is stronger. This observation was consistent with the shorter $M-O_L$ bonds. $\nabla^2\rho$(BCP) < 0 was considered a sufficient nonessential condition for covalent bonding. Theoretically, a partial covalent bond could be indicated by the electron energy density (H) at the bond critical point (BCP). This bond could be considered as covalent interaction for H(BCP) < 0 and noncovalent interaction for >0.

Table S2 shows that negative H values were present in the Am−N bonds of $[ML_2]^{3+}$, $[ML_2(H_2O)]^{3+}$, and $[ML_2(H_2O)_2]^{3+}$. On the contrary, all other bonds exhibited positive H values. The value of |V(BCP)|/G(BCP) served as the criterion for determining the type of bonding: values <1

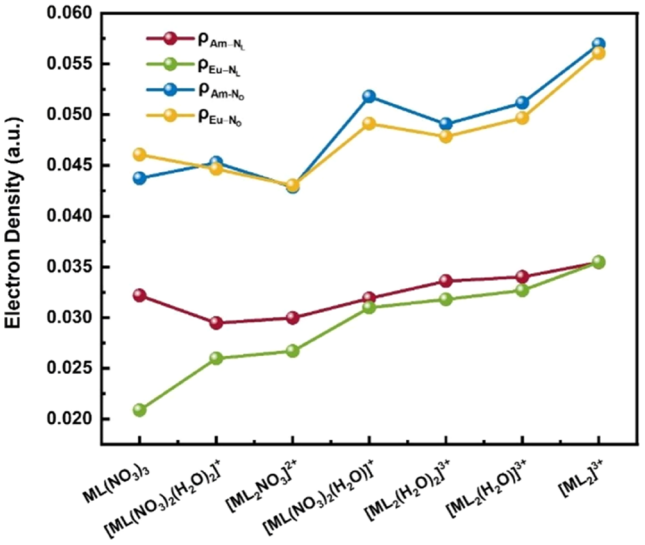

Figure 6. Variation of the calculated average QTAIM parameters ρ at M−O and M−N bonds' BCPs.

indicated closed-shell layer interaction; values >1 but <2 indicated intermediate interaction; and values >2 signified covalent interaction. For the three Am complexes with |V(BCP)|/G(BCP) values <1, which correspond to the negative H values in the table, the Am−N bonds were classified as closed-shell layer interactions, and the others were intermediate interactions. Bond degree (BD), represented by H(r)/ρ(r), measures the energy per unit electron relative to the density at the bond critical point (BCP). For covalent interactions (usually characterized by H(BCP) < 0), a more negative BD indicates a stronger effect. In contrast, for noncovalent interactions (usually H(BCP) > 0), a more positive BD suggests a weaker effect. The data from the table indicate that the Am−N bond exhibited more covalent properties than the rest of the bonds, consistent with the dominant electrostatic interactions obtained from MBOs and WBIs analysis.

The analysis conducted above indicated that the superior Am/Eu separation capability of the bipyridyl phosphate ligands

https://doi.org/10.1021/acsomega.3c09940
ACS Omega 2024, 9, 12060−12068

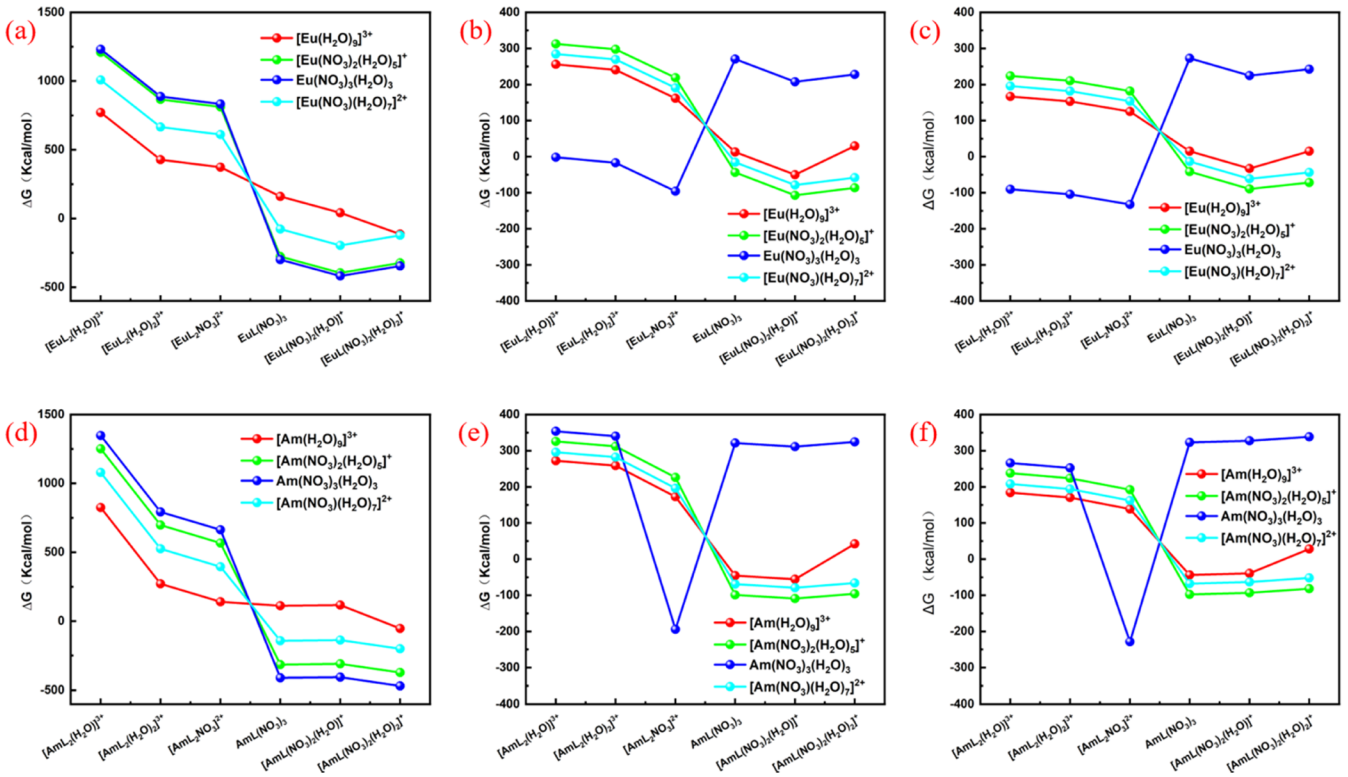

Figure 7. Gibbs free energy changes (ΔG, kcal mol^{-1}) for the 24 complexation interactions of four different Am(III)/Eu(III) starting materials with six different products in water(a,d), cyclohexanone(b,e), and nitrobenzene(c,f) solutions.

Table 3. Gibbs Free Energy Alteration for Am^{3+}/Eu^{3+} Complexes in Aqueous ($\Delta G_{aq}(Am^{3+}/Eu^{3+})$, kcal mol^{-1}), and the Difference of Gibbs Free Energy Alteration between Am^{3+} and Eu^{3+} Complexes ($\Delta\Delta G_{aq/cyc/nit} = \Delta G_{aq/cyc/nit}(Am^{3+}) - \Delta G_{aq/cyc/nit}(Eu^{3+})$, kcal mol^{-1}) in Aqueous, Cyclohexanone, and Nitrobenzene Phases at the B3LYP/6-311G*/RECP Level of Theory

reactions	$\Delta G_{aq.}$	$\Delta\Delta G_{aq.}$	$\Delta\Delta G_{cyc.}$	$\Delta\Delta G_{nit.}$
$[M(NO_3)_2(H_2O)_5]^+ + 2L = [ML_2(H_2O)_2]^{3+} + 2NO_3^- + 3H_2O$	697.47/865.72	−168.26	14.80	13.96
$[M(NO_3)_2(H_2O)_5]^+ + 2L = [ML_2(H_2O)_2]^{3+} + 2NO_3^- + 4H_2O$	1251.90/1208.35	43.55	13.04	14.11
$[M(NO_3)_2(H_2O)_5]^+ + 2L = [ML_2NO_3]^{2+} + NO_3^- + 5H_2O$	567.24/811.10	−243.86	−55.38	10.25
$[M(NO_3)_2(H_2O)_5]^+ + L = [ML(NO_3)2(H_2O)_2]^+ + 3H_2O$	−316.01/−277.27	−50.36	−9.64	−10.13
$[M(NO_3)_2(H_2O)_5]^+ + L + NO_3^- = ML(NO_3)_3 + 5H_2O$	−373.48/−323.12	−38.75	7.47	−55.97
$[M(NO_3)_2(H_2O)_5]^+ + L = [ML(NO_3)_2(H_2O)]^+ + 4H_2O$	−310.67/−396.30	85.63	−2.06	−3.65
$[M(NO_3)(H_2O)7]^{2+} + 2L^+ = [ML_2(H_2O)_2]^{3+} + 5H_2O + NO_3^-$	524.65/665.50	−140.85	12.92	12.08
$[M(NO_3)(H_2O)7]^{2+} + 2L = ML_2(H_2O)^{3+} + 6H_2O + NO_3^-$	1079.08/1008.12	70.96	11.16	12.23
$[M(NO_3)(H_2O)7]^{2+} + 2L = [ML_2NO_3]^{2+} + 7H_2O$	394.41/610.87	−216.45	5.59	8.37
$[M(NO_3)(H_2O)7]^{2+} + L + NO_3^- = [ML(NO_3)_2(H_2O)_2]^+ + 5H_2O$	−143.19/−77.04	−77.77	−7.75	−8.25
$[M(NO_3)(H_2O)7]^{2+} + L + 2NO_3^- = ML(NO_3)_3 + 7H_2O$	−200.66/−122.90	−66.15	−53.50	−54.08
$[M(NO_3)(H_2O)7]^{2+} + L + NO_3^- = [ML(NO_3)_2(H_2O)]^+ + 6H_2O$	−137.85/−196.07	58.23	−0.18	−1.77

was probably due to the moderately greater covalent attributes of the Am−N bond compared to those of the Eu−N bond.

3.4. Energy Analysis. The relationship between bipyridyl phosphate ligands and Am(III) and Eu(III) cations was further investigated based on a thermodynamic perspective. The alteration in Gibbs free energy (ΔG) was computed for 24 probable reactions at the B3LYP/6-311G*/RECP level of theory to evaluate the thermodynamic feasibility of these reactions. The reaction is enthalpy-driven, and ΔG is obtained by subtracting the energies of the reactants from the energies of the products. The reactions were initiated with four reactants, namely, $[M(NO_3)_n(H_2O)_m]^{(3-n)+}$ (M = Am,Eu; n = 1,2,3; m = 7,5,3) and $[M(H_2O)_9]^{3+}$, yielding six different products, namely, $[ML_2(H_2O)]^{3+}$, $[ML_2(H_2O)_2]^{3+}$, $[ML_2NO_3]^{2+}$, $[ML(NO_3)_2H_2O]^+$, $[ML(NO_3)_2(H_2O)_2]^+$, and $ML(NO_3)_3$. The more negative the ΔG is, the lower the system's Gibbs free energy, indicating a greater likelihood of the reaction occurring.

The process of liquid−liquid distribution of Am(III) or Eu(III) ions between nitric acid solution and the organic phase was relatively intricate.[36] The solvation impacts of water, cyclohexanone, and nitrobenzene solutions were taken into account to model potential solvent extraction methods. In the system studied, it was clear that the reactions that gave the $[ML(NO_3)_2H_2O]^+$, $[ML(NO_3)_2(H_2O)_2]^+$ products which had smaller ΔG values (Figure 7). For example, in cyclohexanone solutions of Am(III) and Eu(III) complexes, the values were −99.12 and −43.73 kcal mol^{-1}, respectively. Am complexes

https://doi.org/10.1021/acsomega.3c09940
ACS Omega 2024, 9, 12060−12068

showed higher negative ΔG values compared to those of Eu complexes. This means that the reaction of the Am complex is more likely to occur than that of the Eu complex.

The variation in ΔG for 24 possible complexation reactions in water, cyclohexanone, and nitrobenzene solutions of various starting reactants but the same end products was analyzed. The difference in ΔG between the same products obtained using the initial reactant $[Am(NO_3)_2(H_2O)_5]^+$ with 9 coordination and the initial reactant $Am(NO_3)_3(H_2O)_3$ with 9 coordination numbers was very significant. Thus, it was inferred that decreasing the amount of nitrate in the initial reactants favored the extraction of metal ions, which indicated that nitrate did not promote these reactions. The addition of one water molecule to the initial reactant had a very small effect on ΔG compared with adding one nitrate. Hence, regulating the quantity of nitrate present in the initial reactants affected the extraction process. Nevertheless, in the aqueous solution, a higher concentration of nitrates in the product resulted in more favorable reactions.

Next, the difference in ΔG between Am(III) and Eu(III) complexes ($\Delta\Delta G$) was calculated to compare the thermodynamic favorability of Am(III) and Eu(III) complexation, using the following equation: $\Delta\Delta G_{Am/Eu} = \Delta G_{Am} - \Delta G_{Eu}$,[37] which showed the changes in the ΔG of the Am(III) and Eu(III) compounds produced by each reaction. Most of the $\Delta\Delta G_{aq}$ reactions were negative, which implied that the complexation of the bipyridine phosphate ligand with Am^{3+} was more favorable in energy than with Eu^{3+} and that the reaction of Am(III) was more likely to occur than the Eu(III) reaction (Table 3). It should be noted that our results, in terms of ΔG and $\Delta\Delta G_{Am/Eu}$, are more negative compared to previous studies using bipyridine ligands,[38] indicating a better extraction efficiency for actinide elements. The ΔG values for 1:2 type extraction complexes were mostly positive, while those for 1:1 type extraction complexes were mostly negative. For example, the ΔG values for the reactions in aqueous and nitrobenzene solutions were −373.48 and −81.86 kcal mol^{-1}, corresponding to more negative values than those for the reactions of the 1:2 extraction complexes in aqueous and nitrobenzene solutions. However, the values of $\Delta\Delta G$ for the 1:1 extraction reactions were greater than those of the 1:2 extraction reactions. Therefore, the 1:1 extraction reaction was more effective for the separation of Am(III)/Eu(III). These results showed that optimal separation of Am(III)/Eu(III) cations with bipyridyl phosphate ligands could be accomplished by generating 1:1 type extraction complexes through the modulation of experimental conditions, such as the molar ratio of ligands and metal ions, pH, and temperature. Thus, the study established a theoretical foundation and provided direction for conducting experiments.

4. CONCLUSIONS

We investigated the extraction mechanisms of Am(III) and Eu(III) complexes with a bipyridine phosphate ligand using DFT calculations and analyzed their coordination modes of the complexes through bond length comparisons. Our findings indicate that the coordination of cations is profoundly influenced by the presence of nitrogen and oxygen atoms within the bipyridine phosphate ligands. Owing to oxygen's higher electronegativity relative to nitrogen, all $M-O_L$ bonds are stronger than $M-N_L$ bonds. Furthermore, the presence of oxygen ligands not only reduces the sensitivity of the extractant to acidity but also provides sites for metal coordination, facilitating the separation of lanthanides and actinides even at lower concentrations. In addition, in all examined Am and Eu complexes, nitrate ions formed a bidentate coordination with Am(III) and Eu(III). The Am−N bond is notably shorter and demonstrated a higher WBI value compared with the Eu−N bond, suggesting stronger binding between the ligand and Am(III). Both NBO and QTAIM analyses indicated that the M−N bond exhibits a degree of weak covalent characteristics, while the Am−N bond shows greater covalency than the Eu−N bond.

Based on the thermodynamic analysis, the majority of $\Delta\Delta G_{Am/Eu}$ reactions in the aqueous solution had a negative value. This indicated that the bipyridyl phosphate ligand was selective for Am(III). However, from an energy perspective, compared with cyclohexanone, the separation process in an aqueous solution appeared to be more unfavorable. Based on the changes in ΔG, it was observed that the selection of initial reactants had a notable influence on reaction energetics. Reducing the amount of nitrate in the initial reactants facilitated the extraction of metal ions, indicating that nitrate did not promote these reactions. The reactions in the aqueous solution became more favorable with an increasing amount of nitrate in the product. The formation of $[ML(NO_3)_2(H_2O)_2]^+$ complexes was accompanied by a small change in Gibbs free energy.

Therefore, in order to facilitate the complex formation of Am^{3+} and Eu^{3+} with ligands, it is necessary to control the amount of nitrates in both the initial reactants and products. The phosphorus−oxygen-bonded ligand is more likely to coordinate with the Am element, successfully achieving the goal of separating the actinide element Am from the lanthanide element Eu. The results indicate that the use of the bipyridine phosphate ligand has great potential for the effective separation of An(III)/Ln(III) in spent fuel reprocessing experiments.

■ ASSOCIATED CONTENT

Supporting Information

The Supporting Information is available free of charge at https://pubs.acs.org/doi/10.1021/acsomega.3c09940.

ESP plots for the optimized bipyridine phosphate ligand (Figure S1); maps of HOMO and LUMO of bipyridine phosphate ligand (Figure S2); mean bond lengths of M−N and M−O (Table S1); and calculated averages for four QTAIM parameters of M−N and M−O (Table S2) (PDF)

■ AUTHOR INFORMATION

Corresponding Authors

Miaogen Chen − *Key Laboratory of Intelligent Manufacturing Quality Big Data Tracing and Analysis of Zhejiang Province, College of Science, China Jiliang University, Hangzhou 310018, China;* orcid.org/0000-0003-1930-8331; Email: phycmg@cjlu.edu.cn

Pinwen Huang − *Zhejiang University of Water Resources and Electric Power, Hangzhou 310018, China;* Email: ndhuangpw@gmail.com

Authors

Xinyi Zhang − *Key Laboratory of Intelligent Manufacturing Quality Big Data Tracing and Analysis of Zhejiang Province, College of Science, China Jiliang University, Hangzhou 310018, China*

https://doi.org/10.1021/acsomega.3c09940
ACS Omega 2024, 9, 12060−12068

Lulu Ye − *Key Laboratory of Intelligent Manufacturing Quality Big Data Tracing and Analysis of Zhejiang Province, College of Science, China Jiliang University, Hangzhou 310018, China*

Weihao Chen − *Key Laboratory of Intelligent Manufacturing Quality Big Data Tracing and Analysis of Zhejiang Province, College of Science, China Jiliang University, Hangzhou 310018, China*

Xiaofei Zhang − *Key Laboratory of Intelligent Manufacturing Quality Big Data Tracing and Analysis of Zhejiang Province, College of Science, China Jiliang University, Hangzhou 310018, China*

Weiwei Chen − *Key Laboratory of Intelligent Manufacturing Quality Big Data Tracing and Analysis of Zhejiang Province, College of Science, China Jiliang University, Hangzhou 310018, China*

Complete contact information is available at: https://pubs.acs.org/10.1021/acsomega.3c09940

Notes

The authors declare no competing financial interest.

■ ACKNOWLEDGMENTS

This work was supported by the National Key R&D Program of China (no. 2019YFE0112000), the National Natural Science Foundation of China (no. 22276175), the Zhejiang Xinmiao Talents Program of China (no. 2023R409A050), and the Student Research Program of China Jiliang University (no. 2023X26090). Computational resources were provided by Zhejiang University.

■ REFERENCES

(1) Bodvarsson, G. S.; Boyle, W.; Patterson, R.; Williams, D. Overview of scientific investigations at Yucca Mountain—the potential repository for high-level nuclear waste. *J. Contam. Hydrol.* **1999**, *38*, 3−24.

(2) Chapron, S.; Marie, C.; Pacary, V.; Duchesne, M.-T.; Arrachart, G.; Pellet-Rostaing, S.; Miguirditchian, M. J. P. C. Separation of americium by liquid-liquid extraction using diglycolamides water-soluble complexing agents. *Procedia Chem.* **2016**, *21*, 133−139.

(3) Malinina, T. V.; Murina, V. I.; Medvedeva, L. N.; Yakovlev, D. Y.; Yushkov, E. S. Organizational and Economic Solutions to Create Facilities for Storing and Reprocessing Spent Nuclear Fuel. *At. Energy* **2019**, *126*, 59−61.

(4) Natarajan, R. Reprocessing of spent nuclear fuel in India: present challenges and future programme. *Prog. Nucl. Energy* **2017**, *101*, 118−132.

(5) Croff, A. G. ORIGEN2: A Versatile Computer Code for Calculating the Nuclide Compositions and Characteristics of Nuclear Materials. *Nucl. Technol.* **1983**, *62*, 335−352.

(6) Yapici, H.; Genc, G.; Demir, N. A comprehensive study on neutronics of a lead−bismuth eutectic cooled accelerator-driven sub-critical system for long-lived fission product transmutation. *Ann. Nucl. Energy* **2008**, *35*, 1264−1273.

(7) Serp, J.; Poinssot, C.; Bourg, S. Assessment of the Anticipated Environmental Footprint of Future Nuclear Energy Systems. Comparison between closed and open fuel cycle. *Energies* **2017**, *10*, No. 1445, DOI: 10.3390/en10091445.

(8) Zhang, H. L.; Li, A.; Li, K.; Wang, Z. P.; Xu, X. C.; Wang, Y. X.; Sheridan, M. V.; Hu, H. S.; Xu, C.; Alekseev, E. V.; Zhang, Z. Y.; Yan, P.; Cao, K. C.; Chai, Z. F.; Albrecht-Schönzart, T. E.; Wang, S. A. Ultrafiltration separation of Am(VI)-polyoxometalate from lanthanides. *Nature* **2023**, *616*, 482−487.

(9) Bessen, N.; Yan, Q.; Pu, N.; Chen, J.; Xu, C.; Shafer, J. Extraction of the trivalent transplutonium actinides americium through einsteinium by the sulfur donor Cyanex 301. *Inorg. Chem. Front.* **2021**, *8*, 4177−4185.

(10) Wang, X.; Li, J.; Dai, S.; Hayat, T.; Alsaedi, A.; Wang, X. Interactions of Eu(III) and ^{243}Am(III) with humic acid-bound γ-Al_2O_3 studied using batch and kinetic dissociation techniques. *Chem. Eng. J.* **2015**, *273*, 588−594.

(11) Anshul, K.; Selvakumar, J.; Srinivasan, S.; Suneel, G.; Jawahar, N. R.; Gayen, J. K.; Ravi, K. V. Chromatography separation of minor actinides from Ln^{3+} rich high-level radioactive liquid waste (HLW) using bis-triazinyl-pyridine (BTP) resin. *Sep. Sci. Technol.* **2023**, 2631−2640, DOI: 10.1080/01496395.2023.2223757.

(12) Zhu, Y.; Chen, J.; Jiao, R. Extraction of Am (III) and Eu (III) from nitrate solution with purified Cyanex 301. *Solvent Extr. Ion Exch.* **1996**, *14*, 61−68, DOI: 10.1080/07366299608918326.

(13) Aneheim, E.; Ekberg, C.; Fermvik, A.; Foreman, M.; Grűner, B.; Hajkova, Z.; Kvičalová, M. A TBP/BTBP-based GANEX separation process—part 2: ageing, hydrolytic, and radiolytic stability. *Solvent Extr. Ion Exch.* **2011**, *29*, 157−175.

(14) Ekberg, C.; Löfström-Engdahl, E.; Aneheim, E.; Foreman, M. R. S.; Geist, A.; Lundberg, D.; Denecke, M.; Persson, I. The structures of CyMe 4-BTBP complexes of americium (III) and europium (III) in solvents used in solvent extraction, explaining their separation properties. *Dalton Trans.* **2015**, *44*, 18395−18402.

(15) Lewis, F. W.; Hudson, M. J.; Harwood, L. M. Development of highly selective ligands for separations of actinides from lanthanides in the nuclear fuel cycle. *Synlett* **2011**, *2011*, 2609−2632.

(16) Zsabka, P.; Van Hecke, K.; Adriaensen, L.; Wilden, A.; Modolo, G.; Verwerft, M.; Binnemans, K.; Cardinaels, T. Selective extraction of trivalent actinides using CyMe4BTPhen in the ionic liquid Aliquat-336 nitrate. *RSC Adv.* **2021**, *11*, 6014−6021.

(17) Xu, L.; Pu, N.; Li, Y.; Wei, P.; Sun, T.; Xiao, C.; Chen, J.; Xu, C. Selective Separation and Complexation of Trivalent Actinide and Lanthanide by a Tetradentate Soft−Hard Donor Ligand: Solvent Extraction, Spectroscopy, and DFT Calculations. *Inorg. Chem.* **2019**, *58*, 4420−4430.

(18) Yang, X.; Xu, L.; Hao, Y.; Meng, R.; Zhang, X.; Lei, L.; Xiao, C. Effect of Counteranions on the Extraction and Complexation of Trivalent Lanthanides with Tetradentate Phenanthroline-Derived Phosphonate Ligands. *Inorg. Chem.* **2020**, *59*, 17453−17463.

(19) Xu, L.; Yang, X.; Wang, Z.; Wang, S.; Sun, M.; Xu, C.; Zhang, X.; Lei, L.; Xiao, C. Unfolding the Extraction and Complexation Behaviors of Trivalent f-Block Elements by a Tetradentate N,O-Hybrid Phenanthroline Derived Phosphine Oxide Ligand. *Inorg. Chem.* **2021**, *60*, 2805−2815.

(20) Trumm, S.; Geist, A.; Panak, P. J.; Fanghänel, T. An improved hydrolytically-stable bis-triazinyl-pyridine (BTP) for selective actinide extraction. *Solvent Extr. Ion Exch.* **2011**, *29*, 213−229.

(21) Bulmer, R.; Spencer, T. B.; Wilden, A.; Modolo, G.; Vu, T. H.; Simonin, J. P.; Lewis, F. W. New route to amide-functionalized N-donor ligands enables improved selective solvent extraction of trivalent actinides. *Chem. Commun.* **2022**, *58*, 10667−10670.

(22) Wu, H.; Wu, Q. Y.; Wang, C. Z.; Lan, J. H.; Liu, Z. R.; Chai, Z. F.; Shi, W. Q. Theoretical insights into the separation of Am(III) over Eu(III) with PhenBHPPA. *Dalton Trans.* **2015**, *44*, 16737−16745.

(23) Lee, C.; Yang, W.; Parr, R. G. Development of the Colle-Salvetti correlation-energy formula into a functional of the electron density. *Phys. Rev. B* **1988**, *37*, No. 785, DOI: 10.1103/PhysRevB.37.785.

(24) Becke, A. D. Density-functional exchange-energy approximation with correct asymptotic behavior. *Phys. Rev. A* **1988**, *38*, No. 3098, DOI: 10.1103/PhysRevA.38.3098.

(25) Chapleski, R. C.; Ivanov, A. S.; Peterson, K. A.; Bryantsev, V. S. Improving the theoretical description of Ln (iii)/An (iii) separation with phosphinic acid ligands: a benchmarking study of structure and selectivity. *Phys. Chem. Chem. Phys.* **2021**, *23*, 19558−19570.

(26) Cao, X.; Dolg, M. Segmented contraction scheme for small-core actinide pseudopotential basis sets. *J. Mol. Struct.* **2004**, *673*, 203−209.

(27) Cao, X.; Dolg, M. Segmented contraction scheme for small-core lanthanide pseudopotential basis sets. *J. Mol. Struct.* **2002**, *581*, 139−147.
(28) Lu, T.; Chen, F. Multiwfn: A multifunctional wavefunction analyzer. *J. Comput. Chem.* **2012**, *33*, 580−592.
(29) Klamt, A.; Jonas, V.; Bürger, T.; Lohrenz, J. C. Refinement and parametrization of COSMO-RS. *J. Phys. Chem. A* **1998**, *102*, 5074−5085.
(30) Thakur, P.; Conca, J. L.; Choppin, G. R. Mixed Ligand Complexes of Am^{3+}, Cm^{3+} and Eu^{3+} with HEDTA and HEDTA^{+} NTA—Complexation Thermodynamics and Structural Aspects. *J. Solution Chem.* **2012**, *41*, 599−615.
(31) Ribár, B.; Kapor, A.; Argay, G.; Kálmán, A. Tetraaquatrinitratoeuropium (III) monohydrate. *Acta Crystallogr., Sect. C: Cryst. Struct. Commun.* **1986**, *42*, 1450−1452.
(32) Huang, P.-W.; Wang, C.-Z.; Wu, Q.-Y.; Lan, J.-H.; Song, G.; Chai, Z.-F.; Shi, W.-Q. Theoretical studies on the synergistic extraction of Am^{3+} and Eu^{3+} with CMPO−HDEHP and CMPO−HEH [EHP] systems. *Dalton Trans.* **2018**, *47*, 5474−5482.
(33) Arnold, P. L.; Turner, Z. R.; Kaltsoyannis, N.; Pelekanaki, P.; Bellabarba, R. M.; Tooze, R. P. Covalency in Ce^{IV} and U^{IV} Halide and N-Heterocyclic Carbene Bonds. *Chem. - Eur. J.* **2010**, *16*, 9623−9629.
(34) Kerridge, A. Quantification of f-element covalency through analysis of the electron density: insights from simulation. *Chem. Commun.* **2017**, *53*, 6685−6695.
(35) Fryer-Kanssen, I.; Austin, J.; Kerridge, A. Topological Study of Bonding in Aquo and Bis(triazinyl)pyridine Complexes of Trivalent Lanthanides and Actinides: Does Covalency Imply Stability? *Inorg. Chem.* **2016**, *55*, 10034−10042.
(36) Petit, L.; Joubert, L.; Maldivi, P.; Adamo, C. A comprehensive theoretical view of the bonding in actinide molecular complexes. *J. Am. Chem. Soc.* **2006**, *128*, 2190−2191.
(37) Narbutt, J.; Wodyński, A.; Pecul, M. The selectivity of diglycolamide (TODGA) and bis-triazine-bipyridine (BTBP) ligands in actinide/lanthanide complexation and solvent extraction separation − a theoretical approach. *Dalton Trans.* **2015**, *44*, 2657−2666.
(38) G, A. J.; Ebenezer, C.; Solomon, R.V. Selective complexation of trivalent americium over europium with substituted Triazolebipyridine-based ligand in high Level-Liquid Waste- A DFT Investigation. *Polyhedron* **2022**, *220*, No. 115832, DOI: 10.1016/j.poly.2022.115832.

https://doi.org/10.1021/acsomega.3c09940
ACS Omega 2024, 9, 12060−12068